

Nanoneedle-Electrode Devices for *In Vivo* Recording of Extracellular Action Potentials

Tomoaki Banno, Shuhei Tsuruhara, Yu Seikoba, Ryohei Tonai, Koji Yamashita, Shinnosuke Idogawa, Yuto Kita, Ko Suzuki, Yuki Yagi, Yuki Kondo, Rika Numano, Kowa Koida, and Takeshi Kawano*



Cite This: *ACS Nano* 2022, 16, 10692–10700



Read Online

ACCESS |



Metrics & More



Article Recommendations

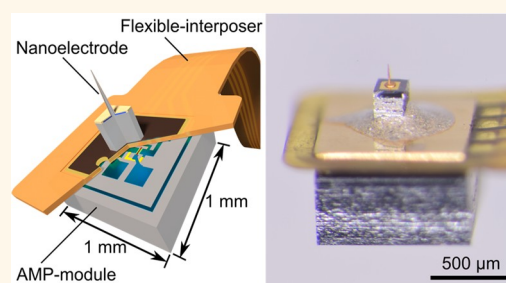


Supporting Information

ABSTRACT: Microscale needle-like electrode technologies offer *in vivo* extracellular recording with a high spatiotemporal resolution. Further miniaturization of needles to nanoscale minimizes tissue injuries; however, a reduced electrode area increases electrical impedance that degrades the quality of neuronal signal recording. We overcome this limitation by fabricating a 300 nm tip diameter and 200 μm long needle electrode where the amplitude gain with a high-impedance electrode ($>15\text{ M}\Omega$, 1 kHz) was improved from 0.54 (-5.4 dB) to 0.89 (-1.0 dB) by stacking it on an amplifier module of source follower. The nanoelectrode provided the recording of both local field potential ($<300\text{ Hz}$) and action potential ($>500\text{ Hz}$) in the mouse cortex, in contrast to the electrode without the amplifier.

These results suggest that microelectrodes can be further minimized by the proposed amplifier configuration for low-invasive recording and electrophysiological studies in submicron areas in tissues, such as dendrites and axons.

KEYWORDS: nanoelectrode, MOSFETs, extracellular recording, neuron, electrophysiology



INTRODUCTION

Microscale needle-like electrode devices penetrated into brain tissue have made significant contributions to neuroscience in terms of recording neuronal activity with a high spatiotemporal resolution. Microscale fabrication technology typically known as silicon-based “Michigan Probe”^{1–3} and “Utah array”^{4–6} miniaturizes the device geometry and enables an increase in the number of electrodes. These device technologies have been expanded further to the large number of recording sites realized by complementary metal-oxide-semiconductor (CMOS) technology.^{7,8} However, such electrode devices involve a rigid needle-shaped electrode material (e.g., silicon or metal) with a diameter (or width) of $>20\text{ }\mu\text{m}$, which forms a hole in the tissue and causes tissue injuries.^{9,10}

Foreign object (e.g., needle-like electrode)-induced injuries in biological tissue (e.g., brain tissue) must be minimized in order to observe the nature of neuronal activities, particularly in electrophysiological recording *in vivo*. Several device strategies to minimize tissue injury have been proposed, such as a thin needle with a flexible substrate, solving a mismatch in elasticity between the needle electrode and soft brain tissues.^{11–15} A needle electrode with a diameter of $<10\text{ }\mu\text{m}$ minimizes tissue injuries.¹⁶ Such small needles have been fabricated for *in vivo* recording from carbon fiber ($<8.6\text{ }\mu\text{m}$,¹⁷ $8.4\text{ }\mu\text{m}$ ¹⁸) and silicon needle ($<7\text{ }\mu\text{m}$,^{19,20} $<5\text{ }\mu\text{m}$ ²¹) technologies. These electrode devices are used in the brain tissue, the spinal cord,²² and the peripheral nervous

system,^{23–25} offering a “neural interface” having the advantages of low invasiveness and stable recording of these neuronal activities. Nanowire device technologies also contribute to the neural recording; however, these nanodevices have been limited to *in vivo* recording in terms of a short electrode length of $<100\text{ }\mu\text{m}$.^{26–29} This issue of nanodevices was overcome with a fabrication process of a $>100\text{ }\mu\text{m}$ long nanoscale sharpened microneedle electrode involving the growth of silicon microneedle and the subsequent tip-sharpening process.^{30–32} The nanoelectrode penetrated the brain tissue of mice and demonstrated *in vivo* extracellular recording of low-frequency signals ($<300\text{ Hz}$) of local field potential (LFP). However, no high-frequency signals ($>500\text{ Hz}$) of the action potential (detected as unit or spike activity) were recorded because the small electrode area of below $7.7\text{ }\mu\text{m}^2$ induced a high impedance.³³

The nanoelectrode electrical properties at a high-frequency range can be improved by an impedance transformation with amplifier (AMP). Recently, we proposed a single needle

Received: March 11, 2022

Accepted: June 9, 2022

Published: July 5, 2022



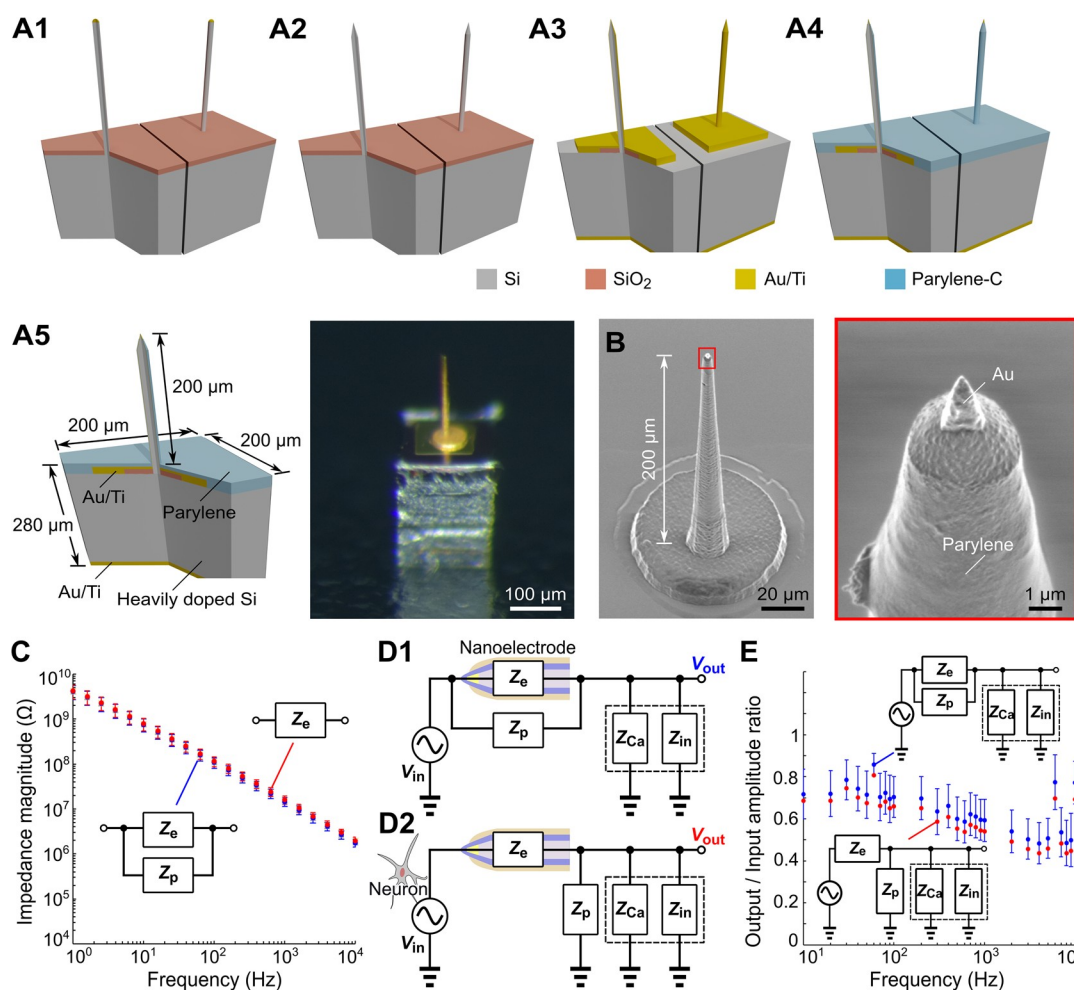


Figure 1. Nanoneedle-electrode device. (A1–A4) Fabrication of nanoneedle electrode device (see the Supporting Information for the details). (A5) Schematic and photograph of a nanoneedle-electrode device. The nanoneedle was fabricated in the center of a $200 \times 200 \mu\text{m}^2$ conductive Si substrate with the thickness of $280 \mu\text{m}$. (B) SEM images of a $200 \mu\text{m}$ long nanoneedle electrode. The red square depicts the needle tip comprising the $<300 \text{ nm}$ diameter gold tip visible over the parylene insulating layer. (C) Magnitudes of electrical impedance of nine nanoneedle-electrode devices measured in PBS at room temperature. The graph involves the experimentally measured impedance (system with parallel needle electrolyte/metal interfacial impedance, Z_e and parylene layer-induced parasitic device impedance, Z_p) and the calculated electrode impedance (Z_e). (D) Equivalent circuit diagrams for the test signal recording in PBS (D1) and the neural recording in the amplifier, Z_{in} . The parasitic device impedance, Z_p , which is connected in parallel to the electrode impedance, Z_e , in the test signal recording, is grounded in the neural recording. (E) O/I signal-amplitude ratios of the nanoneedle-electrode device in the test signal recording (blue) and the neural recording (red). The O/I ratios of test signal recording were measured in PBS at room temperature. Means and standard deviations are taken from eight devices. The O/I ratios in the neural recording (red) were calculated with the ratios taken from the test signal recording (blue).

topped amplifier package, called STACK, involving a $1 \times 1 \text{ mm}^2$ size AMP module consisting of source follower (SF) stacked on a microneedle electrode device;³⁴ herein, the same packaging technology is applied to the nanoelectrode. The nanoneedle electrode with a needle length of $200 \mu\text{m}$ is fabricated on a $200 \times 200 \mu\text{m}^2$ substrate by the growth of silicon microneedle and its sharpening. The electrical properties are improved by assembling the electrode with the AMP module. The nanoelectrode with AMP demonstrates the *in vivo* extracellular recording of mice neuronal activity.

RESULTS AND DISCUSSION

The nanoneedle electrode was fabricated by sharpening a microneedle electrode²¹ to the nanoscale using a method reported in the previous study³⁰ (Figure 1A1–A4, see details in Figure S1). The silicon microneedle electrode was fabricated

by gold-catalyzed vapor–liquid–solid growth.³⁵ The microscale needle tip was sharpened to nanoscale by silicon chemical etching.^{30,33} After the device metallization with gold, a highly biocompatible insulating layer of parylene-C was deposited on the device surface, and the tip section of the needle was oxygen plasma etched.^{31,32} Electrode device modules were separated by a laser-dicing process. Figure 1A5,B demonstrates the fabricated nanoneedle-electrode device. Scanning microscope (SEM) images represent a fabricated $200 \mu\text{m}$ long nanoneedle electrode with the gold tip (Figure 1B). The tip curvature radius is $\sim 150 \text{ nm}$, and its height over the parylene insulating layer is $\sim 3.3 \mu\text{m}$ (the parylene thickness is $1.35 \mu\text{m}$). The die size of the device fabricated for *in vivo* neural recording in mouse brain tissue was $200 \mu\text{m} \times 200 \mu\text{m}$.

We characterized the fabricated nanoneedle electrode, which has a recording area of $\sim 7 \mu\text{m}^2$ made of gold at the tip portion.

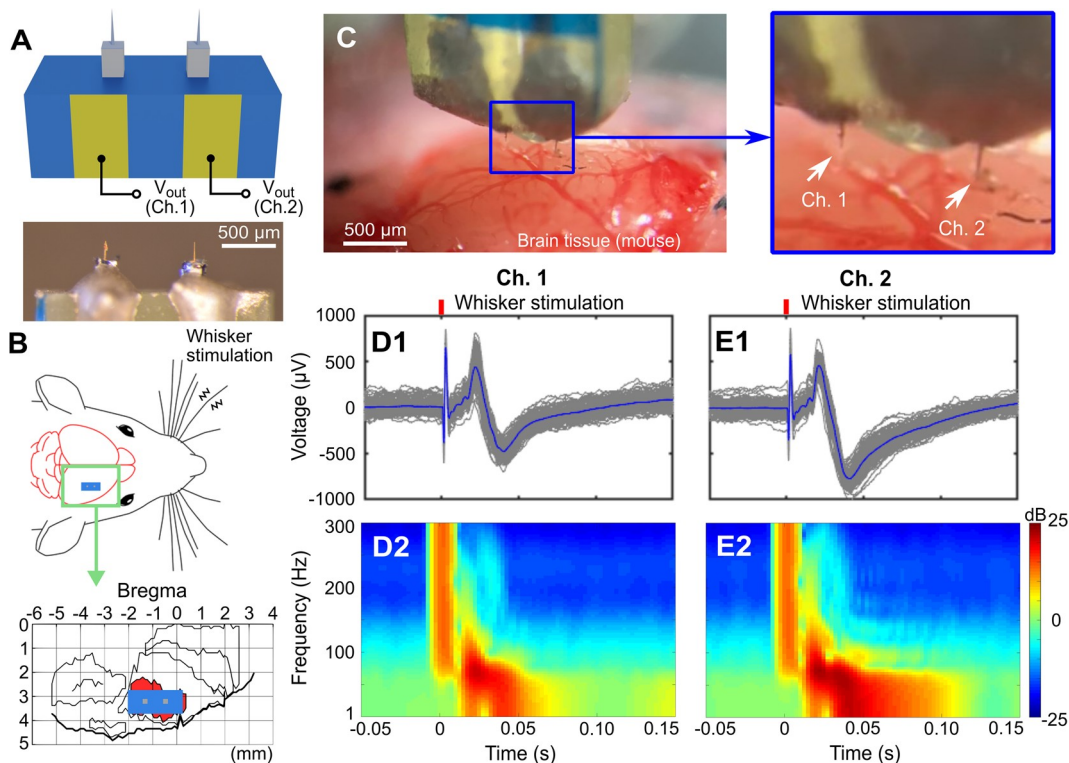


Figure 2. *In vivo* recording of signals in the mouse cortex with nanoneedle electrode devices. (A) Schematic and photograph of two nanoneedle-electrode devices assembled on a PCB. The distance between the nanoneedles is $\sim 850\ \mu\text{m}$. (B) Schematic representing the positions of the PCB and two nanoneedle electrodes in the primary somatosensory barrel cortex (S1B) of a mouse. (C) Photograph of two nanoneedle electrodes during the penetration. (D, E) Signals simultaneously acquired from the cortical area (S1B) using two nanoneedle electrodes: waveforms of low-frequency band (filtering = 1 to 300 Hz) signals via Ch.1 electrode (D1) and Ch.2 electrode (E1) and time-frequency spectrograms of signals via Ch.1 (D2) and Ch.2 (E2). Waveforms appeared at 0 to 0.01 s correspond to stimulation-induced artifacts.

The nanoneedle electrode showed impedance magnitudes ranging from 23.7 k Ω to 4.14 G Ω at 1 Hz–10 kHz (14.7 M Ω at 1 kHz for action potential recording, averaged for $n = 9$ nanoneedle electrodes measured in phosphate-buffered saline (PBS) at room temperature, blue scatters in Figure 1C). Because the measured impedance includes both the electrode impedance, Z_e , and the parylene-induced parasitic device impedance, Z_p (Figure S2), the electrode impedance can be derived by subtracting the parasitic impedance.³² Given the parasitic device impedance (Z_p) of 168 M Ω at 1 kHz, the electrode impedance at 1 kHz is 16.1 M Ω (red scatters in Figure 1C).

Output/input (O/I) signal amplitude ratios of the fabricated nanoneedle electrode with the recording system were measured to confirm the recorded neuronal signal attenuation associated with the nanoneedle electrode and the recording system. The O/I ratios in the neural recording can be derived from the test signal recording and a circuit model (Figure 1D).³² The O/I ratios measured in PBS with a test signal (Figure 1D1) were 48–86% at 10 Hz–10 kHz (59% at 1 kHz, averaged for $n = 8$ nanoneedle electrodes, measured at room temperature, blue scatters in Figure 1E). The O/I ratios decreased during actual neural recording due to the grounded parasitic device impedance (Z_p , Figure 1D2) (Supporting Information).^{32,36} Considering the grounded parasitic device impedance, the O/I ratios in actual neural recording are 41–81% in the same frequency range ($\sim 54\%$ at 1 kHz for spike recording, red scatters in Figure 1E).

In vivo extracellular recording in mouse brain was performed to confirm the penetrating and recording capabilities of the nanoneedle electrode. Two fabricated nanoneedle-electrode devices were assembled on a printed circuit board (PCB) with conductive epoxy (Figure 2A). The gap between these electrodes was 850 μm . Silicon sidewalls of the electrode device and PCB electrode pads were insulated with resin for the experiments with animals. Mice were anesthetized with an intraperitoneal injection using chlorprothixene and urethane (see the Experimental Section). After removal of the cranium and dura mater (0–2 mm caudal and 2 to 4 mm lateral to the bregma), a two-channel nanoneedle-electrode device was placed on the primary somatosensory barrel cortex (S1B), and the nanoneedles with the length of 200 μm penetrated the area of layer 2/3 (Figure 2B,C). Then the mouse contralateral whiskers were physically stimulated to characterize the evoked neuronal potentials.

These nanoneedle electrodes penetrated the tissue without fracture and detected local field potential (LFP) (filtering = 1–300 Hz, $n = 100$ trials) in the mouse cortex (S1B). The signals were in response to the whisker stimulation with a latency of ~ 20 ms at the onset of the whisker stimuli while showing the peak-to-peak amplitude of $>900\ \mu\text{V}$ averaged by $n = 100$ trials for each channel (Figure 2D1,E1). These waveforms are similar to the LFP recorded by conventional tungsten microelectrode, $\sim 5\text{-}\mu\text{m}$ -diameter silicon-microneedle electrode ($\sim 100\ \text{k}\Omega$ at 1 kHz by platinum black modification), and nanoscale silicon-needle electrode with the same recording system,^{21,33} suggesting that these signals are neuronal

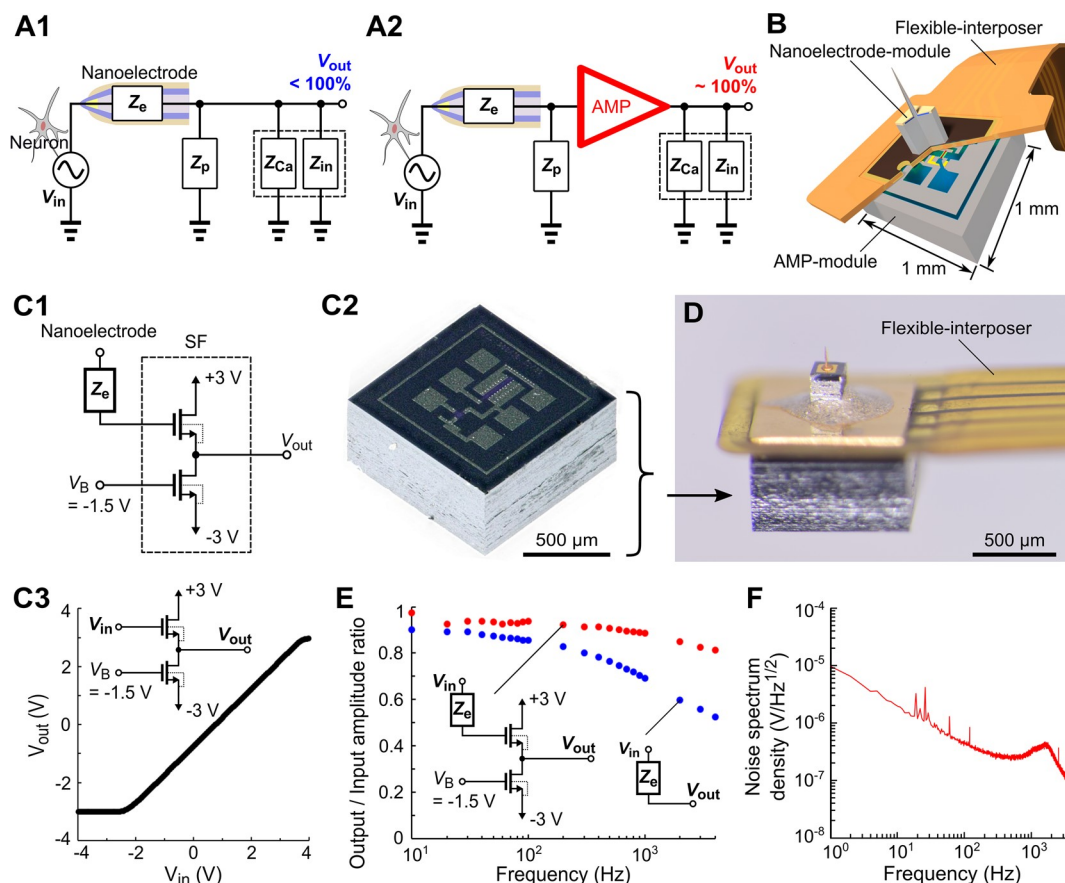


Figure 3. Nano-STACK device. (A) Equivalent circuits of nanoneedle-electrode devices: nanoelectrode without AMP module (A1) and with AMP module (A2). (B) Schematic of the assembled Nano-STACK device. (C) AMP module. (C1) Equivalent circuit of SF design in the AMP module. (C2) Photograph of the AMP module. (C3) Input–output voltage characteristics of the SF in the module with a voltage gain of 0.98 (−0.14 dB). (D) Photograph of the assembled Nano-STACK device. The overall device thickness excluding the nanoneedle portion is ~ 0.9 mm including 280 μm thick needle module, 100 μm thick flexible interposer, and 525 μm thick AMP module. Silicon sidewalls of each module are insulated with resin for subsequent device characterization and experiments involving animals. (E) O/I signal-amplitude ratios of the two types of nanoneedle-electrode devices with (red) and without (blue) the AMP module. The curves were measured in PBS at room temperature by applying sinusoidal test signals with the peak-to-peak amplitude of 100 μV at 10–4000 Hz *via* a counter electrode. (F) Measured voltage noise spectrum densities for the nanoneedle electrode with the AMP module.

responses evoked by the stimuli. In contrast, no high-frequency band (filtering = 500–1000 Hz) signals were recorded with these electrodes in response to the spike activity due to the high electrical impedance characteristics of the nanoneedle electrode (16.1 $\text{M}\Omega$ at 1 kHz) (Figure 2D2,E2).

The high impedance characteristics of the nanoelectrode in the neural recording can be improved by adding an AMP module to the electrode module (Nano-STACK) (Figure 3A). Here, we used our prior packaging technique where the nanoelectrode module was attached to the AMP module *via* a flexible interposer (Figure 3B).³⁴ As the AMP module, we used a SF of two n-type MOSFETs (NMOS) configuration fabricated in the $1 \times 1 \text{ mm}^2$ area of silicon substrate by aluminum (Al)-interconnection-based in-house 5 μm gate-length NMOS technology (Figure 3C).^{34,37} Gate widths/lengths (W/L) of these drive and load MOSFETs are 200/10 and 15/30 μm , respectively, having an input impedance of 115 $\text{M}\Omega$ (exceeding the electrode impedance of 16.1 $\text{M}\Omega$ at 1 kHz) and an output impedance of 5.5 $\text{k}\Omega$. The input–output voltage ($V_{\text{in}} - V_{\text{out}}$) characteristics of the fabricated SF show the linear dependence with the voltage gain of 0.98 (−0.14 dB) (Figure 3C3).

The fabricated AMP module attached on the nanoneedle electrode improved the electrode impedance. The device was assembled using a flexible interposer of polyimide-based printed circuit (FPC, 100 μm thick). The AMP module was mounted on bottom of the interposer by flip chip bonding with anisotropic conductive paste. The other module of nanoneedle-electrode device was mounted on top of the FPC *via* conductive epoxy (CW2400, CircuitWorks) (Figure 3D).³⁴ The fabricated STACK device has the area of $1 \times 1 \text{ mm}^2$ and the overall thickness of ~ 1 mm. The silicon sidewalls of the STACK device were encapsulated with insulating resin for the animal experiment.

The electrical characteristics of the high-impedance nanoneedle electrode were improved by the stacked AMP module. The fabricated STACK device exhibited the increased O/I signal amplitude ratios of $>80\%$ at 10–4000 Hz (89% at 1 kHz for spike recording) (Figure 3E). The difference in voltage gain between the SF and the STACK device is caused by the voltage attenuation associated with the electrode impedance (Z_e), the parasitic device impedance (Z_p), and the SF input impedance. Figure 3F represents the measured voltage noise spectrum densities of the fabricated STACK device. The peak appearing at ~ 1 kHz is an artifact of the recording system used

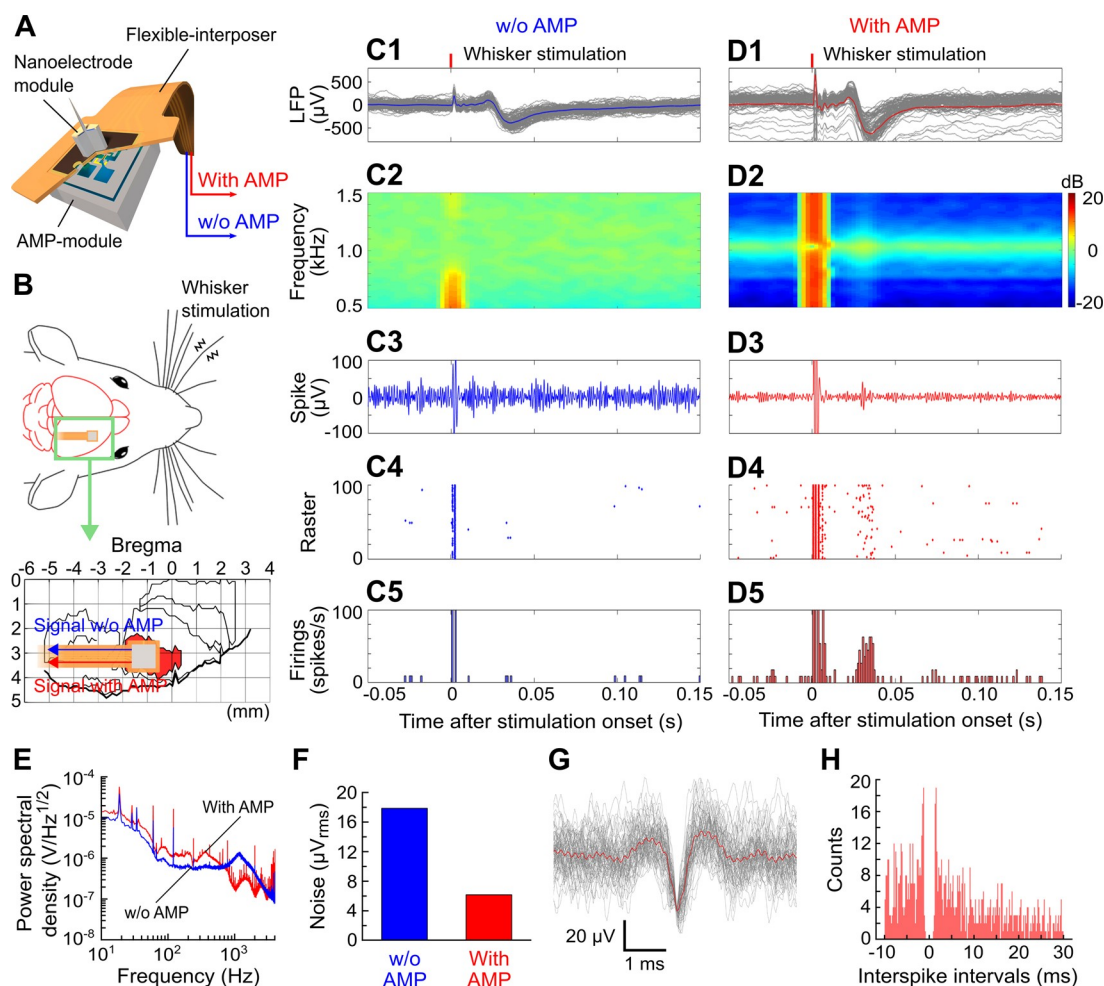


Figure 4. *In vivo* recording of signals in mouse cortex with Nano-STACK device. (A) Schematic of Nano-STACK device with two signal outputs with and without the AMP. (B) Schematic representing the position of the Nano-STACK device on the primary somatosensory barrel cortex (S1B) of the mouse. (C) Sample signals acquired from the cortical area (S1B) with the nanoneedle electrode without the AMP: waveforms of the low-frequency band (filtering = 1–300 Hz, $n = 100$ trials) signals (C1), time-frequency spectrogram (filtering = 500–1500 Hz) of signals (C2), high-frequency band (filtering = 500–1000 Hz) signal waveform from a single trial (C3), raster plot diagrams (C4), and PSTHs based on these signals (C5). (D) Sample signals acquired from the cortical area with the same nanoneedle electrode with the AMP: waveforms of the low-frequency band (filtering = 1–300 Hz, $n = 100$ trials) signals (D1), time-frequency spectrograms (filtering = 500–1500 Hz) of signals (D2), high-frequency band (filtering = 500–1000 Hz) signal waveform from a single trial (D3), raster plot diagrams (D4) and PSTHs based on these signals (D5). (E) PSDs of the recordings using the nanoneedle electrode with and without the AMP. (F) rms noise of the nanoneedle electrode with (red) and without (blue) the AMP. (G) Enlarged waveforms of 147 superimposed spikes taken using the nanoneedle electrode with the AMP (D3–D5) (4σ -amplitude threshold). (H) ISI distribution for these spikes.

(see the [Experimental Section](#)). The voltage noise level in the neuronal activity range (1–1000 Hz in this work) was below 10^{-5} V/Hz^{1/2}. This noise level is acceptable because for the background noise of <10 μ V of the recording system (see the [Experimental Section](#)) and amplitudes of neuronal activity exceeding 10 μ V.

In vivo extracellular recording capability of the fabricated STACK device was demonstrated using mice ([Figure 4](#)). The nanoneedle electrode had two signal outputs with and without the AMP module for comparison of the recorded signals ([Figure 4A](#), [Figure S3](#)). The mice were anesthetized with an intraperitoneal injection using chlorprothixene and urethane. After removal of the cranium and dura mater, the nanoneedle electrode of the STACK device penetrated the mouse cortex (S1B) ([Figure 4B](#)) (refer the [Experimental Section](#)).

The nanoneedle electrode without the AMP module detected evoked LFP (filtering = 1–300 Hz, $n = 100$ trials) by whisker stimulation ([Figure 4C1](#)), while no remarkable

high-frequency signals (filtering = 500–1000 Hz) were observed due to the high electrode impedance ([Figure 4C2–C5](#)). However, the same nanoneedle electrode with the AMP module enabled detection of both the LFP and the high-frequency band signals in this recording session ([Figure 4D1–D5](#)). [Figure 4D3](#) illustrates a typical high-frequency band signal waveform detected with an amplitude threshold of the high-frequency signals, which is $4\times$ the SD (σ) of the mean signal obtained -0.5 to -1.0 s before the stimulus onset. The waveform is similar to that of extracellular spike activity recorded with a conventional tungsten microelectrode and ~ 5 μ m diameter silicon-needle electrodes (~ 100 k Ω at 1 kHz by platinum-black tip modification).²¹ Parts D4 and D5 of [Figure 4](#) demonstrate the raster plot diagrams and the peristimulus time histograms (PSTHs) of the detected high-frequency signals, respectively, while the firing peak appeared at 20 to 40 ms after the stimulus onset. The signal latency is also consistent with sensory responses in mice (S1B) recorded

with conventional electrodes.²¹ These results suggested that the high-frequency signals represented the neuronal spike activity evoked by mouse whisker stimulation. Additional recording sessions with other samples also demonstrated the same ability to detect the spike activity with the AMP module (Figure S4).

Recorded data were further analyzed with and without the AMP module (Figure 4E). The power spectrum densities (PSD) of the nanoneedle electrode without the AMP module are flat at >100 Hz, suggesting that thermal noise is dominant because of a high electrode impedance (the peak at ~1 kHz is an artifact of the recording system used; see the Experimental Section). This PSD property is consistent with the high-frequency signal recording where no significant spikes were detected (4σ amplitude threshold, Figure 4C3–C5). Comparing the frequency ranges, the nanoelectrode with the AMP module exhibits higher PSD at 100–600 Hz. Although the PSD with AMP is lower at >600 Hz, these signals are not significantly affected by noise as confirmed at high-frequency signal recording (Figure 4D3–D5). The noise level in the high-frequency band of 500–1000 Hz was compared with and without AMP module by measuring the signals 0.5–1 s before the stimulus onset. The measured root-mean-square (rms) noise, V_{rms} , with the AMP module in the high-frequency range was $6.2 \mu\text{V}_{\text{rms}}$, while the noise of $17.9 \mu\text{V}_{\text{rms}}$ was observed without the AMP (Figure 4F). Figure 4G represents 147 superimposed spikes from the AMP stacked nanoneedle electrode (4σ amplitude threshold), showing the peak-to-peak amplitude of $53.1 \mu\text{V}$ with the peak-to-peak time of 0.57 ms. Figure 4H represents the interspike intervals (ISI) with the peak amplitude at 1.4 ms, suggesting that the detected spikes corresponded to multiunit activity (signals originated from multiple neurons).

We fabricated a nanoneedle electrode with a length of 200 μm , which enables us to reach neurons in layers 2/3 of the mouse cortex. For animals larger than mice, e.g., rats and monkeys, longer needles are necessary to approach the corresponding cell layers in the tissues. The needle can be elongated by increasing the growth time with the growth rate (1.2 $\mu\text{m}/\text{min}$ at ~750 °C).³⁵ On the other hand, <200 μm long nanoneedle electrodes fabricated at reduced growth time are applicable to *in vitro* and *ex vivo* biological samples, such as cultured neurons and brain slices.

In *in vivo* electrophysiological recording within the brain tissue, the size of a foreign object (e.g., needle electrode in this study) must be miniaturized to observe the nature of neuronal activities without fracturing the biological system. We overcame this issue by fabricating a nanoneedle electrode having a tip diameter of <300 nm. However, the nanoneedle electrode showed the decreased O/I signal amplitude ratios at >100 Hz because of high electrode impedance characteristics.²⁰ Each needle electrode has a gold nanoscale tip with an area of ~7 μm^2 , showing the impedance of 16.1 M Ω and the degraded O/I signal amplitude ratio of 54% at 1 kHz. These electrode characteristics disabled the recording of high-frequency spike components (>500 Hz). The proposed SF configuration by a packaging technique enabled the spike recording with the O/I ratio improved up to 89% while achieving the spikes recorded. Another candidate to improve the O/I ratio is to decrease the electrode impedance by increasing needle tip area and height up to >7.7 μm^2 and >3.5 μm , respectively, by oxygen plasma etching (Figure 1B).³² However, the increased tip area degrades the spatial resolution.

The impedance can be reduced as well without increasing the nanotip area by using a low-impedance material instead of gold, e.g., iridium oxide (IrOx)³⁸ and poly(3,4-ethylenedioxythiophene) (PEDOT).³⁹ The combination of a low-impedance electrode with the stacking AMP configuration may also improve the O/I ratio. The SF configuration also contributed to the noise reduction in the recording system. The nanoelectrode stacked with the AMP module yielded a noise level of $6.2 \mu\text{V}_{\text{rms}}$ during the recording, while the noise of the same electrode without the AMP module was $17.9 \mu\text{V}_{\text{rms}}$. The noise may be further reduced by using low-noise transistors, such as a p-channel MOSFET or bipolar transistor.

In vivo neural recording in mouse cortex was demonstrated with either one- (with AMP) or two-channel (without AMP) nanoneedle electrode devices. For the application of the nanoelectrode with AMP to multichannel recording, the number of nanoelectrodes may be increased by arranging them on a flexible interposer, while the AMP module involves an array of SFs for each channel of electrode. With the same STACK device area of ~1 × 1 mm², a 2 × 2 array of four nanoelectrodes can be arranged with the nanoelectrode device (200 × 200 μm^2 substrate). We have also reported the fabrication of the nanoelectrode array device within the single silicon substrate of 2 × 8.75 mm².³³ These device technologies offer *in vivo* multichannel neural recording within the tissue using nanoscale electrodes.

The nanoscale area of the electrode enables intracellular recording. We have demonstrated an *in vivo* intracellular recording. However, the intracellular action potentials were not recorded due to the degraded O/I signal amplitude ratio of 50% at 1 kHz associated with the electrode impedance of 4.74 M Ω .³³ The proposed Nano-STACK device with a high O/I ratio will be applied to recordings of both intracellular action potentials and postsynaptic potentials, providing insight into fundamental mechanisms in brain and nervous systems *in vivo*.

CONCLUSION

The high impedance of the nanoscale electrode device, which degraded the spike recording capability, was improved by stacking the AMP module of the SF configuration. The improved electrical characteristics enabled us to detect *in vivo* extracellular signals of both LFP and spike activity in mice. Such an approach reduces the electrode impedance, providing opportunities for further electrode miniaturization, thus leading to the next generation of *in vivo* electrophysiology addressing submicroscale areas in tissues, such as dendrites and axons.⁴⁰

EXPERIMENTAL SECTION

Ethics. All experimental procedures were approved by the Committee for the Use of Animals at Toyohashi University of Technology, and all animal care followed the Standards Relation to the Care and Management of Experimental Animals (Notification No. 6, 27 March 1980 of the Prime Minister's Office of Japan).

Silicon Needle Growth. Microscale-diameter vertical silicon needles were fabricated on a (111) silicon substrate by the gold-catalyzed vapor–liquid–solid (VLS) growth. The catalytic gold dot was placed on the silicon surface by evaporation and photoresist-based lift-off processes. The silicon needle fabrication involves placing the substrate in a gas-source molecular-beam epitaxy chamber and conducting the VLS growth of silicon at a growth temperature of ~750 °C to grow individual silicon needles from these gold dots. A mixture of 1% phosphine (PH₃) (diluted in 99% hydrogen) with 100% disilane (Si₂H₆) was the source of silicon gas.³⁵ The needle

length was controlled by maintaining a constant growth rate of 1.2 $\mu\text{m}/\text{min}$. Polycrystalline Si deposited from vapor phase over the substrate during the VLS growth was removed with the etching gas [xenon difluoride (XeF_2)].

Electrical Characterization. The electrolyte/metal interfacial impedance of the electrode was measured in PBS solution at room temperature by applying a test sinusoidal wave with a peak-to-peak amplitude of 100 mV at 1–1000 Hz via a counter electrode of stainless. Impedance measurements were performed using an impedance analyzer (Model 1260A Impedance/Gain-Phase Analyzer, Solartron Analytical, UK). The output/input (O/I) signal amplitude ratios of the electrode with the recording system were analyzed in PBS at room temperature by applying input sinusoidal test signals with a peak-to-peak amplitude of 100 μV at 1–1000 Hz via a counter electrode (stainless). The output signals were amplified using a recording amplifier (ZC64, Tucker-Davis Technologies, USA, input resistance = $1 \times 10^{14} \Omega$). The signals recorded through the amplifier were routed to a preamplifier/digitizer (PZ2, Tucker-Davis Technologies) and acquired with a digital signal-processing module (RZ2, Tucker-Davis Technologies).

In Vivo Recording. The extracellular recording capability of the fabricated nanoneedle-electrode device was verified by *in vivo* recording the local field potential and spike activity of mouse cerebral cortex. We used mice (male, 22–31 g in weight) anesthetized using intraperitoneal injection of chlorprothixene (100 μL of 0.5% solution per 10 g body weight) and urethane (50 μL of 10% solution per 10 g body weight). Using a manipulator, the nanoneedle electrode device was placed on the exposed primary somatosensory cortex (S1B) of the mouse, and the electrode penetrated the brain tissue. The penetration was confirmed by microscopy.

For *in vivo* extracellular recording in mouse brain, the fabricated nanoneedle-electrode device packaged with either a printed circuit board (PCB) or a flexible printed circuit (FPC) was connected to a recording amplifier (ZC64, Tucker-Davis Technologies, USA, input impedance = $1 \times 10^{14} \Omega$). The signals recorded through the amplifier were routed to a preamplifier/digitizer (PZ2, Tucker-Davis Technologies, USA) and acquired with a digital signal-processing module (RZ2, Tucker-Davis Technologies, USA).

The mouse whiskers were mechanically stimulated during the recording to activate the S1B with a vibrating stimulation system driven by 1 ms duration pulse signals from processing system (RZ2, Tucker-Davis Technologies, USA). The stimulus intensity was manually adjusted to enable observation of the neuronal activity with an interstimulus interval of 3 s. The stimulating signals were synchronized to acquire the neuronal signals using the same processing system.

ASSOCIATED CONTENT

Supporting Information

The Supporting Information is available free of charge at <https://pubs.acs.org/doi/10.1021/acsnano.2c02399>.

Fabrication of nanoneedle electrode module, parasitic impedance system, cross-sectional view of Nano-STACK device, and *in vivo* recording using other set of samples and Nano-STACK device (Figures S1–S4) (PDF)

AUTHOR INFORMATION

Corresponding Author

Takeshi Kawano – Department of Electrical and Electronic Information Engineering, Toyohashi University of Technology, Toyohashi, Aichi 441-8580, Japan; Electronics-Inspired Interdisciplinary Research Institute, Toyohashi University of Technology, Toyohashi, Aichi 441-8580, Japan; orcid.org/0000-0003-1535-9254; Email: kawano@ee.tut.ac.jp

Authors

- Tomoaki Banno** – Department of Electrical and Electronic Information Engineering, Toyohashi University of Technology, Toyohashi, Aichi 441-8580, Japan
- Shuhei Tsuruhara** – Department of Electrical and Electronic Information Engineering, Toyohashi University of Technology, Toyohashi, Aichi 441-8580, Japan
- Yu Seikoba** – Department of Electrical and Electronic Information Engineering, Toyohashi University of Technology, Toyohashi, Aichi 441-8580, Japan
- Ryohei Tonai** – Department of Electrical and Electronic Information Engineering, Toyohashi University of Technology, Toyohashi, Aichi 441-8580, Japan
- Koji Yamashita** – Electronics-Inspired Interdisciplinary Research Institute, Toyohashi University of Technology, Toyohashi, Aichi 441-8580, Japan
- Shinnosuke Idogawa** – Department of Electronic engineering, National Institute of Technology, Kushiro College, Kushiro, Hokkaido 084-0916, Japan
- Yuto Kita** – Department of Electrical and Electronic Information Engineering, Toyohashi University of Technology, Toyohashi, Aichi 441-8580, Japan
- Ko Suzuki** – TechnoPro R&D Company, Minatoku, Tokyo 106-6135, Japan
- Yuki Yagi** – Department of Electrical and Electronic Information Engineering, Toyohashi University of Technology, Toyohashi, Aichi 441-8580, Japan
- Yuki Kondo** – Department of Electrical and Electronic Information Engineering, Toyohashi University of Technology, Toyohashi, Aichi 441-8580, Japan
- Rika Numano** – Electronics-Inspired Interdisciplinary Research Institute and Applied Chemistry and Life Science, Toyohashi University of Technology, Toyohashi, Aichi 441-8580, Japan
- Kowa Koida** – Electronics-Inspired Interdisciplinary Research Institute and Department of Computer and Science and Engineering, Toyohashi University of Technology, Toyohashi, Aichi 441-8580, Japan

Complete contact information is available at: <https://pubs.acs.org/doi/10.1021/acsnano.2c02399>

Author Contributions

T.K. designed the research. T.B., S.T., Y.S., S.I., Y.Ki., K.S., Y.Y., and Y.Ko. prepared the devices. T.B., S.T., Y.S., Y.Ki., S.I., and Y.Ko. performed the device characterizations. T.B., R.T., K.Y., and Y.Ko. conducted the animal experiment. T.B., R.T., K.Y., R.N., K.K., and T.K. analyzed the data. T.B. and T.K. wrote the manuscript. T.K. supervised the project.

Notes

The authors declare no competing financial interest.

ACKNOWLEDGMENTS

We acknowledge support from Japan Society for the Promotion of Science (JSPS) Grants-in-Aid for Scientific Research (KAKENHI) Grant Nos. 17H03250, 26709024, and 20H00244, the Strategic Advancement of Multi-Purpose Ultra-Human Robot and Artificial Intelligence Technologies program from the New Energy and Industrial Technology Development Organization (NEDO), Adaptable and Seamless Technology transfer Program through Target-driven R&D (A-STEP) from Japan Science and Technology Agency (JST) and Nagai Foundation for Science & Technology. R.N. was

supported by Takeda Science Foundation. K.K. was supported by JSPS KAKENHI Grant Nos. 15H05917 and 20H00614.

REFERENCES

- (1) Najafi, K.; Wise, K. D.; Mochizuki, T. A High-Yield IC-Compatible Multichannel Recording Array. *IEEE Trans. Electron Devices* **1985**, *32* (7), 1206–1211.
- (2) Najafi, K.; Ji, J.; Wise, K. D. Scaling Limitations of Silicon Multichannel Recording Probes. *IEEE Transactions on Biomedical Engineering* **1990**, *37* (1), 1–11.
- (3) Bai, Q.; Wise, K. D.; Anderson, D. J. A High-Yield Microassembly Structure for Three-Dimensional Microelectrode Arrays. *IEEE Transactions on Biomedical Engineering* **2000**, *47* (3), 281–289.
- (4) Campbell, P. K.; Jones, K. E.; Huber, R. J.; Horch, K. W.; Normann, R. A. A Silicon-Based, Three-Dimensional Neural Interface: Manufacturing Processes for an Intracortical Electrode Array. *IEEE Trans Biomed Eng.* **1991**, *38* (8), 758–768.
- (5) Rousche, P. J.; Normann, R. A. A Method for Pneumatically Inserting an Array of Penetrating Electrodes into Cortical Tissue. *Annals of Biomedical Engineering* **1992**, *20* (4), 413–422.
- (6) Rousche, P. J.; Normann, R. A. Chronic Recording Capability of the Utah Intracortical Electrode Array in Cat Sensory Cortex. *Journal of Neuroscience Methods* **1998**, *82* (1), 1–15.
- (7) Jun, J. J.; Steinmetz, N. A.; Siegle, J. H.; Denman, D. J.; Bauza, M.; Barbarits, B.; Lee, A. K.; Anastassiou, C. A.; Andrei, A.; Aydin, Ç.; Barbic, M.; Blanche, T. J.; Bonin, V.; Couto, J.; Dutta, B.; Gratiy, S. L.; Gutnisky, D. A.; Häusser, M.; Karsh, B.; Ledochowitsch, P.; Lopez, C. M.; Mittelut, C.; Musa, S.; Okun, M.; Pachitariu, M.; Putzeys, J.; Rich, P. D.; Rossant, C.; Sun, W.; Svoboda, K.; Carandini, M.; Harris, K. D.; Koch, C.; O’Keefe, J.; Harris, T. D. Fully Integrated Silicon Probes for High-Density Recording of Neural Activity. *Nature* **2017**, *551* (7679), 232–236.
- (8) Obaid, A.; Hanna, M. E.; Wu, Y. W.; Kollo, M.; Racz, R.; Angle, M. R.; Müller, J.; Brackbill, N.; Wray, W.; Franke, F.; Chichilnisky, E. J.; Hierlemann, A.; Ding, J. B.; Schaefer, A. T.; Melosh, N. A. Massively Parallel Microwire Arrays Integrated with CMOS Chips for Neural Recording. *Science Advances* **2020**, *6* (12). DOI: 10.1126/sciadv.aay2789.
- (9) Szarowski, D. H.; Andersen, M. D.; Retterer, S.; Spence, A. J.; Isaacson, M.; Craighead, H. G.; Turner, J. N.; Shain, W. Brain Responses to Micro-Machined Silicon Devices. *Brain Res.* **2003**, *983* (1–2), 23–35.
- (10) Chen, R.; Canales, A.; Anikeeva, P. Neural Recording and Modulation Technologies. *Nature Reviews Materials* **2017**, *2* (2), 1–16.
- (11) Takeuchi, S.; Suzuki, T.; Mabuchi, K.; Fujita, H. 3D Flexible Multichannel Neural Probe Array. *Journal of Micromechanics and Microengineering* **2004**, *14* (1), 104.
- (12) Kim, B. J.; Kuo, J. T. W.; Hara, S. A.; Lee, C. D.; Yu, L.; Gutierrez, C. A.; Hoang, T. Q.; Pikov, V.; Meng, E. 3D Parylene Sheath Neural Probe for Chronic Recordings. *Journal of Neural Engineering* **2013**, *10* (4), 045002.
- (13) Liu, J.; Fu, T.-M.; Cheng, Z.; Hong, G.; Zhou, T.; Jin, L.; Duvvuri, M.; Jiang, Z.; Kruskal, P.; Xie, C.; Suo, Z.; Fang, Y.; Lieber, C. M. Syringe-Injectable Electronics. *Nat. Nanotechnol.* **2015**, *10* (July), 629–636.
- (14) Musk, E. Neuralink. An Integrated Brain-Machine Interface Platform with Thousands of Channels. *bioRxiv* **2019**, 703801.
- (15) Luan, L.; Wei, X.; Zhao, Z.; Siegel, J. J.; Potnis, O.; Tuppen, C. A.; Lin, S.; Kazmi, S.; Fowler, R. A.; Holloway, S.; Dunn, A. K.; Chitwood, R. A.; Xie, C. Ultraflexible Nanoelectronic Probes Form Reliable, Glial Scar-Free Neural Integration. *Science Advances* **2017**, *3* (2), No. e1601966.
- (16) Edell, D. J.; Toi, V. V.; McNeil, V. M.; Clark, L. D. Factors Influencing the Biocompatibility of Insertable Silicon Microshafts in Cerebral Cortex. *IEEE Transactions on Biomedical Engineering* **1992**, *39* (6), 635–643.
- (17) Kozai, T. D. Y.; Langhals, N. B.; Patel, P. R.; Deng, X.; Zhang, H.; Smith, K. L.; Lahann, J.; Kotov, N. A.; Kipke, D. R. Ultrasmall Implantable Composite Microelectrodes with Bioactive Surfaces for Chronic Neural Interfaces. *Nat. Mater.* **2012**, *11* (12), 1065–1073.
- (18) Patel, P. R.; Na, K.; Zhang, H.; Kozai, T. D. Y.; Kotov, N. A.; Yoon, E.; Chestek, C. A. Insertion of Linear 8.4 Mm Diameter 16 Channel Carbon Fiber Electrode Arrays for Single Unit Recordings. *J. Neural Eng.* **2015**, *12* (4), 046009.
- (19) Fujishiro, A.; Kaneko, H.; Kawashima, T.; Ishida, M.; Kawano, T. A Penetrating Micro-Scale Diameter Probe Array for in Vivo Neuron Spike Recordings. In *2011 IEEE 24th International Conference on Micro Electro Mechanical Systems*; IEEE, 2011; pp 1011–1014. DOI: 10.1109/MEMSYS.2011.5734599.
- (20) Fujishiro, A.; Kaneko, H.; Kawashima, T.; Ishida, M.; Kawano, T. In Vivo Neuronal Action Potential Recordings via Three-Dimensional Microscale Needle-Electrode Arrays. *Sci. Rep.* **2015**, *4*, 4868.
- (21) Sawahata, H.; Yamagiwa, S.; Moriya, A.; Dong, T.; Oi, H.; Ando, Y.; Numano, R.; Ishida, M.; Koida, K.; Kawano, T. Single 5 μm Diameter Needle Electrode Block Modules for Unit Recordings in Vivo. *Sci. Rep.* **2016**, *6* (1), 35806.
- (22) Mineev, I. R.; Musienko, P.; Hirsch, A.; Barraud, Q.; Wenger, N.; Moraud, E. M.; Gandar, J.; Capogrosso, M.; Milekovic, T.; Asboth, L.; Torres, R. F.; Vachicouras, N.; Liu, Q.; Pavlova, N.; Duis, S.; Larmagnac, A.; Vörös, J.; Micera, S.; Suo, Z.; Courtine, G.; Lacour, S. P. Electronic Dura Mater for Long-Term Multimodal Neural Interfaces. *Science (1979)* **2015**, *347* (6218), 159–163.
- (23) Wang, J.; He, T.; Lee, C. Development of Neural Interfaces and Energy Harvesters towards Self-Powered Implantable Systems for Healthcare Monitoring and Rehabilitation Purposes. *Nano Energy* **2019**, *65*, 104039.
- (24) Cho, Y.; Park, J.; Lee, C.; Lee, S. Recent Progress on Peripheral Neural Interface Technology towards Bioelectronic Medicine. *Bioelectronic Medicine* **2020**, *6* (1), 23.
- (25) Shin, H.; Kang, M.; Lee, S. Mechanism of Peripheral Nerve Modulation and Recent Applications. *International Journal of Optomechatronics* **2021**, *15* (1), 182–198.
- (26) Tian, B.; Cohen-Karni, T.; Qing, Q.; Duan, X.; Xie, P.; Lieber, C. M. Three-Dimensional, Flexible Nanoscale Field-Effect Transistors as Localized Bioprobes. *Science (1979)* **2010**, *329* (5993), 830–834.
- (27) Hai, A.; Shappir, J.; Spira, M. E. In-Cell Recordings by Extracellular Microelectrodes. *Nat. Methods* **2010**, *7* (3), 200–202.
- (28) Robinson, J. T.; Jorgolli, M.; Shalek, A. K.; Yoon, M.-H. H.; Gertner, R. S.; Park, H. Vertical Nanowire Electrode Arrays as a Scalable Platform for Intracellular Interfacing to Neuronal Circuits. *Nat. Nanotechnol.* **2012**, *7* (3), 180–184.
- (29) Abbott, J.; Ye, T.; Qin, L.; Jorgolli, M.; Gertner, R. S.; Ham, D.; Park, H. CMOS Nanoelectrode Array for All-Electrical Intracellular Electrophysiological Imaging. *Nat. Nanotechnol.* **2017**, *12* (5), 460–466.
- (30) Goryu, A.; Ikedo, A.; Ishida, M.; Kawano, T. Nanoscale Sharpening Tips of Vapor-Liquid-Solid Grown Silicon Microwire Arrays. *Nanotechnology* **2010**, *21* (12), 125302.
- (31) Goryu, A.; Numano, R.; Ikedo, A.; Ishida, M.; Kawano, T. Nanoscale Tipped Microwire Arrays Enhance Electrical Trap and Depth Injection of Nanoparticles. *Nanotechnology* **2012**, *23* (41), 415301.
- (32) Kubota, Y.; Oi, H.; Sawahata, H.; Goryu, A.; Ando, Y.; Numano, R.; Ishida, M.; Kawano, T. Nanoscale-Tipped High-Aspect-Ratio Vertical Microneedle Electrodes for Intracellular Recordings. *Small* **2016**, *12* (21), 2846–2853.
- (33) Kubota, Y.; Yamagiwa, S.; Sawahata, H.; Idogawa, S.; Tsuruhara, S.; Numano, R.; Koida, K.; Ishida, M.; Kawano, T. Long Nanoneedle-Electrode Devices for Extracellular and Intracellular Recording in Vivo. *Sensors and Actuators, B: Chemical* **2018**, *258*, 1287–1294.
- (34) Kita, Y.; Tsuruhara, S.; Kubo, H.; Yamashita, K.; Seikoba, Y.; Idogawa, S.; Sawahata, H.; Yamagiwa, S.; Leong, X. L. A.; Numano, R.; Koida, K.; Kawano, T. Three-Micrometer-Diameter Needle

Electrode with an Amplifier for Extracellular in Vivo Recordings. *Proc. Natl. Acad. Sci. U. S. A.* **2021**, *118* (16), e2112240119 DOI: 10.1073/pnas.2008233118.

(35) Ikedo, A.; Kawashima, T.; Kawano, T.; Ishida, M. Vertically Aligned Silicon Microwire Arrays of Various Lengths by Repeated Selective Vapor-Liquid-Solid Growth of n-Type Silicon/n-Type Silicon. *Appl. Phys. Lett.* **2009**, *95* (3), 033502.

(36) Harimoto, T.; Takei, K.; Kawano, T.; Ishihara, A.; Kawashima, T.; Kaneko, H.; Ishida, M.; Usui, S. Enlarged Gold-Tipped Silicon Microprobe Arrays and Signal Compensation for Multi-Site Electroretinogram Recordings in the Isolated Carp Retina. *Biosens. Bioelectron.* **2011**, *26* (5), 2368.

(37) Okugawa, A.; Mayumi, K.; Ikedo, A.; Ishida, M.; Kawano, T. Heterogeneously Integrated Vapor-Liquid-Solid Grown Silicon Probes/(111) and Silicon MOSFETs/(100). *IEEE Electron Device Lett.* **2011**, *32* (5), 683–685.

(38) Yamagiwa, S.; Fujishiro, A.; Sawahata, H.; Numano, R.; Ishida, M.; Kawano, T. Layer-by-Layer Assembled Nanorough Iridium-Oxide/Platinum-Black for Low-Voltage Microscale Electrode Neurostimulation. *Sens. Actuators, B* **2015**, *206*, 205–211.

(39) Cui, X.; Martin, D. C. Electrochemical Deposition and Characterization of Poly(3,4-Ethylenedioxythiophene) on Neural Microelectrode Arrays. *Sens. Actuators, B* **2003**, *89* (1–2), 92–102.

(40) Patolsky, F.; Timko, B. P.; Yu, G.; Fang, Y.; Greytak, A. B.; Zheng, G.; Lieber, C. M. Detection, Stimulation, and Inhibition of Neuronal Signals with High-Density Nanowire Transistor Arrays. *Science* (1979) **2006**, *313* (5790), 1100–1104.

Recommended by ACS

Porous Polyethylene Terephthalate Nanotemplate Electrodes for Sensitive Intracellular Recording of Action Potentials

Dongxin Xu, Ning Hu, *et al.*

MARCH 07, 2022
NANO LETTERS

READ 

3D Diamond Electrode Array for High-Acuity Stimulation in Neural Tissue

Melanie E. M. Stamp, David J. Garrett, *et al.*

FEBRUARY 09, 2020
ACS APPLIED BIO MATERIALS

READ 

Electrochemical Evaluation of Layer-by-Layer Drug Delivery Coating for Neural Interfaces

Kaitlynn P. Olczak, Kevin J. Otto, *et al.*

NOVEMBER 13, 2019
ACS APPLIED BIO MATERIALS

READ 

Nanotunnels within Poly(3,4-ethylenedioxythiophene)-Carbon Nanotube Composite for Highly Sensitive Neural Interfacing

Nuan Chen, Nitish V. Thakor, *et al.*

JUNE 24, 2020
ACS NANO

READ 

Get More Suggestions >